Atmos. Chem. Phys. Discuss., 13, 10345–10393, 2013
www.atmos-chem-phys-discuss.net/13/10345/2013/
doi:10.5194/acpd-13-10345-2013

Atmospheric Chemistry and Physics Discussions

Quantitative determination of carbonaceous particle mixing state in Paris using single particle mass spectrometer and aerosol mass spectrometer measurements

R. M. Healy[1,2], J. Sciare[3], L. Poulain[4], M. Crippa[5], A. Wiedensohler[4], A. S. H. Prévôt[5], U. Baltensperger[5], R. Sarda-Estève[3], M. L. McGuire[2], C.-H. Jeong[2], E. McGillicuddy[1], I. P. O'Connor[1], J. R. Sodeau[1], G. J. Evans[2], and J. C. Wenger[1]

[1]Department of Chemistry and Environmental Research Institute, University College Cork, Ireland
[2]Southern Ontario Centre for Atmospheric Aerosol Research, University of Toronto, 200 College Street, Toronto, Ontario, Canada
[3]LSCE, Laboratoire des Sciences du Climat et de l'Environnement, CEA-CNRS-UVSQ, Gif-sur-Yvette, France
[4]Leibniz Institute for Tropospheric Research, Leipzig, Germany
[5]Laboratory of Atmospheric Chemistry, Paul Scherrer Institute, PSI Villigen, 5232, Switzerland

Received: 1 March 2013 – Accepted: 11 April 2013 – Published: 19 April 2013

Correspondence to: R. M. Healy (robert.healy@utoronto.ca)

Published by Copernicus Publications on behalf of the European Geosciences Union.

ACPD
13, 10345–10393, 2013

Abstract

Single particle mixing state information can be a powerful tool for assessing the relative impact of local and regional sources of ambient particulate matter in urban environments. However, quantitative mixing state data are challenging to obtain using single particle mass spectrometers. In this study, the quantitative chemical composition of carbonaceous single particles has been estimated using an aerosol time-of-flight mass spectrometer (ATOFMS) as part of the MEGAPOLI 2010 winter campaign in Paris, France. Relative peak areas of marker ions for elemental carbon (EC), organic aerosol (OA), ammonium, nitrate, sulphate and potassium were compared with concurrent measurements from an Aerodyne high resolution time-of-flight aerosol mass spectrometer (HR-ToF-AMS), a thermal/optical OCEC analyser and a particle into liquid sampler coupled with ion chromatography (PILS-IC). ATOFMS-derived mass concentrations reproduced the variability of these species well (R^2 = 0.67–0.78), and ten discrete mixing states for carbonaceous particles were identified and quantified. Potassium content was used to identify particles associated with biomass combustion. The chemical mixing state of HR-ToF-AMS organic aerosol factors, resolved using positive matrix factorization, was also investigated through comparison with the ATOFMS dataset. The results indicate that hydrocarbon-like OA (HOA) detected in Paris is associated with two EC-rich mixing states which differ in their relative sulphate content, while fresh biomass burning OA (BBOA) is associated with two mixing states which differ significantly in their OA/EC ratios. Aged biomass burning OA (OOA_2-BBOA) was found to be significantly internally mixed with nitrate, while secondary, oxidized OA (OOA) was associated with five particle mixing states, each exhibiting different relative secondary inorganic ion content. Externally mixed secondary organic aerosol was not observed. These findings demonstrate the heterogeneity of primary and secondary organic aerosol mixing states in Paris. Examination of the temporal behaviour and chemical composition of the ATOFMS classes also enabled estimation of the relative contribution of transported emissions of each chemical species and total particle mass in the

ACPD
13, 10345–10393, 2013

size range investigated. Only 22 % of the total ATOFMS-derived particle mass was apportioned to fresh, local emissions, with 78 % apportioned to regional/continental scale emissions.

1 Introduction

Particulate matter is known to impact significantly upon air quality in urban environments, and elevated ambient mass concentrations are associated with adverse health effects (Heal et al., 2012). Megacities, defined as metropolitan areas with populations greater than 10 million inhabitants, have been the focus of several large-scale air quality measurement studies in recent years (Molina et al., 2010; Gao et al., 2011; Harrison et al., 2012b). While poor air quality in megacities is of serious concern at a local scale, the potential impact of the associated urban plumes on the surrounding regions must also be considered. Particulate matter and precursor gas emissions may lead to haze formation or acidic deposition at a regional scale, potentially impacting upon human health and crop production (Chameides et al., 1994; Molina and Molina, 2004; Lawrence et al., 2007).

Summer and winter intensive measurement campaigns were undertaken in Paris, France in 2009/2010 as part of the collaborative project entitled Megacities: emissions, urban, regional and Global Atmospheric POLlution and climate effects, and Integrated tools for assessment and mitigation (MEGAPOLI). These measurements were performed to investigate the impact of the Paris plume upon local, regional and global air quality. However, emissions from outside the city have recently been demonstrated to contribute significantly to ambient particulate matter levels in Paris, particularly during periods influenced by continental air masses (Sciare et al., 2010; Gros et al., 2011; Freutel et al., 2013; Healy et al., 2012; Bressi et al., 2012; Zhang et al., 2012; Crippa et al., 2013a,b).

The different sources of wintertime elemental carbon (EC) and black carbon (BC) in Paris have previously been investigated in detail using aerosol time-of-flight mass

ACPD
13, 10345–10393, 2013

spectrometer (ATOFMS), aethalometer and single particle soot photometer (SP2) measurements (Healy et al., 2012; Favez et al., 2009; Crippa et al., 2013a; Laborde et al., 2012). Local emissions associated with vehicular traffic were found to be the predominant source of EC and BC, followed by domestic biomass combustion. A subsequent study, which focused on the apportionment of organic aerosol (OA) detected by a high resolution aerosol time-of-flight mass spectrometer (HR-ToF-AMS), resolved five factors for OA at an urban background site using positive matrix factorization (PMF) (Crippa et al., 2013a). Primary sources of OA included local vehicle exhaust (11 %), domestic biomass combustion (15 %) and cooking activities (17 %). Secondary, oxidized OA was found to account for a significant fraction of the OA mass (> 50 %), and was associated with mid-to-long range transport. Recent studies have highlighted the importance of regional and continental contributions to particulate inorganic ion and OA mass concentrations in Paris using a variety of chemical composition measurements at multiple sites (Sciare et al., 2010; Bressi et al., 2012; Freutel et al., 2013; Crippa et al., 2013b). Advection of $PM_{2.5}$ (particulate matter with aerodynamic diameter $< 2.5\,\mu m^{-3}$) from Northwestern and Eastern Europe has been associated with poor air quality events in the city (Sciare et al., 2010). Effective assessment of the relative impacts of local and regional/continental emissions is therefore necessary to inform mitigation strategies aimed at preventing future exceedences of EU limit values for annual mean mass concentrations of $PM_{2.5}$ in Paris.

Single particle mass spectrometers are well suited to the association of unique particle classes with specific sources (Reinard et al., 2007; Ault et al., 2010; Healy et al., 2010; Bhave et al., 2001; Bein et al., 2007; Moffet et al., 2008; Pratt and Prather, 2012). However, quantifying the relative contribution of each particle class to ambient particle number and mass concentrations can be difficult. Size-dependent particle detection efficiency and composition-dependent ionization efficiency issues are the predominant confounding factors (Allen et al., 2000; Reilly et al., 2000; Kane and Johnston, 2000; Wenzel et al., 2003). Sizing efficiency scaling curves can be generated using co-located particle sizing instruments (Allen et al., 2000; Qin et al., 2006; Reinard et al.,

ACPD
13, 10345–10393, 2013

2007; Pratt and Prather, 2009), and significant advances have also been made in the quantification of specific chemical species in single particles based on their respective mass spectral ion intensities (Fergenson et al., 2001; Hinz et al., 2005; Ferge et al., 2006; Spencer and Prather, 2006; Zelenyuk et al., 2008; Pratt et al., 2009; Froyd et al., 2010; Jeong et al., 2011a). The addition of light scattering modules to aerosol mass spectrometers represents another step forward in the quantification of non-refractory species at a single particle level (Cross et al., 2007, 2009; Liu et al., 2012). Despite these advances, simultaneous quantitative determination of the refractory and non-refractory chemical composition of single particles remains challenging.

The first aim of this work was to quantitatively determine the chemical composition and mixing state of single particles detected in Paris during the MEGAPOLI winter campaign using an ATOFMS through comparison with concurrent measurements of OA, EC and inorganic ion mass concentrations. The second aim was to use the ATOFMS-derived chemical composition data to estimate the relative contributions of local and regional/continental sources of particulate matter impacting upon air quality in Paris, and to identify potential source regions for transported particles.

2 Methodology

2.1 Sampling site and instrumentation

The sampling site and instrumentation used have been described in detail previously (Healy et al., 2012), but are briefly discussed here. Measurements were performed from 15 January–11 February 2010 at an urban background site at the Laboratoire d'Hygiène de la Ville de Paris (LHVP), Paris (48.75° N, 2.36° E). An ATOFMS (Gard et al., 1997) (TSI model 3800) fitted with an aerodynamic lens (TSI model AFL100) was used to measure the size-resolved chemical composition of single particles in the size range 100–3000 nm (vacuum aerodynamic diameter, d_{va}). Particles were sampled through a stainless steel sampling line from a height of 4 m above ground level.

ACPD
13, 10345–10393, 2013

The operating principles of the instrument are as follows; single particles are sampled through a critical orifice and focused in the aerodynamic lens before transmission to the sizing region where d_{va} for each particle is calculated based on its time-of-flight between two continuous wave lasers (Nd : YAG, 532 nm). Particles are subsequently desorbed/ionized using a Nd : YAG laser (266 nm), and the resultant positive and negative ions are detected using a bipolar time-of-flight mass spectrometer. Thus a dual ion mass spectrum is collected for each particle successfully sized and ionized.

Several instruments were located in a container adjacent to the van housing the ATOFMS, and sampled from a separate inlet. These included an Aerodyne High Resolution Time-of-Flight Aerosol Mass Spectrometer (HR-ToF-AMS) (DeCarlo et al., 2006), and a Twin Differential Mobility Particle Sizer (TDMPS) (Birmili et al., 1999) A collection efficiency of 0.4 was calculated for the HR-ToF-AMS based on comparison with concurrent independent measurements (Crippa et al., 2013a). The instruments were connected to a sampling system consisting of a PM_{10} inlet located approximately 6 m a.g.l. directly followed by an automatic aerosol diffusion dryer system, maintaining relative humidity in the sampling line below 30 % (Tuch et al., 2009).

Elemental carbon (EC) and organic carbon (OC) in $PM_{2.5}$, sampled on the roof of the LHVP building (14 m a.g.l.), were analysed using an OCEC field instrument (Sunset Laboratory, Forest Grove, OR) (Bae et al., 2004) The OCEC analyser was operated at 8 L min^{-1} and provided semi-continuous hourly concentrations of OC and EC. A denuder was placed upstream in order to minimise VOC adsorption artefacts. Measurement uncertainty for this instrument is poorly described in the literature and thus an estimate of 20 % is assumed here (Peltier et al., 2007; Sciare et al., 2011). A particle-into-liquid sampler, coupled to two ion chromatographs (PILS-IC) also sampled $PM_{2.5}$ from the roof of the same building, and was used to determine mass concentrations of inorganic ions including sodium and potassium. The instrument is described in detail elsewhere (Sciare et al., 2011).

ACPD
13, 10345–10393, 2013

Meteorological data were collected using a Campbell Scientific weather station. Additional meteorological data was also provided by Météo-France, collected at Parc Montsouris (48.82° N, 2.34° E, 75 m a.s.l.), approximately 1.5 km from LHVP.

2.2 ATOFMS data analysis

Approximately 1.75 million dual ion single particle mass spectra were collected during the MEGAPOLI winter campaign. Mass spectra were imported into ENCHILADA, a freeware data analysis software package (Gross et al., 2010), clustered using the K-means algorithm (K = 80) and manually regrouped into fifteen final classes (Healy et al., 2012). Ten carbonaceous classes were identified, comprising approximately 1.50 million spectra. The remaining mass spectra were either miscalibrated, dominated by noise, or belonged to classes with minimal contributions to the total particle number (< 2 %).

The total hourly particle counts from the ATOFMS were divided into eight size bins in the size range 150–1067 nm (d_{va}) and then scaled using coincident hourly averaged TDMPS number-size distribution data. This provided size-resolved particle number concentrations for each ATOFMS class, assuming spherical shape and a density of 1.5 g cm^{-3} for all particles as described previously (Healy et al., 2012). The sum of the scaled mass concentrations for the ten carbonaceous classes agreed well with the summed concentrations of EC, OA, ammonium, nitrate, sulphate, chloride, potassium and sodium measured by the other instruments (R^2 = 0.91, N = 501), but the ATOFMS values were consistently lower (slope = 0.81, orthogonal distance regression) as shown in Fig. S1. It should be noted that OA, ammonium, nitrate and sulphate were detected in PM_1 by the HR-ToF-AMS, while EC, sodium and potassium were detected in $PM_{2.5}$ by the OCEC and PILS-IC instruments, respectively. The scaled ATOFMS data only covers the size range 150–1067 nm and this may contribute to the low bias.

The quantitative approach described here is an adaptation of that developed by Jeong et al. (2011a). In that case, the relative peak areas (RPAs) for marker ions assigned to EC, OA, ammonium, nitrate and sulphate were used to directly estimate the

ACPD
13, 10345–10393, 2013

volume fraction of these species in each single particle. Hourly scaling factors were then derived by comparing the total summed volume concentration for each chemical species with concurrent independent measurements.

In this work, a different approach is taken. First, a single number-weighted average mass spectrum for all 1.5 million particles contained in the ten carbonaceous classes was generated (Fig. S2). The following representative marker ions were chosen to represent OA: m/z 27 $[C_2H_3]^+$, 29 $[C_2H_5]^+$, 37 $[C_3H]^+$, 43 $[C_2H_3O]^+$ and EC: m/z 12, 24, 36, 48, 60, 72, 84 $[C_{1-7}]^+$ and m/z −12, −24, −36, −48, −60, −72, −84 $[C_{1-7}]^-$. Similar ions have been used to estimate OA/EC ratios in previous ATOFMS studies (Spencer and Prather, 2006; Su et al., 2006; Ferge et al., 2006; Baeza-Romero et al., 2009; Cahill et al., 2012; Pagels et al., 2013). The following ions were chosen to represent ammonium, sulphate, nitrate and potassium: m/z 18 $[NH_4]^+$, −97 $[HSO_4]^-$, −62 $[NO_3]^-$ and 39 $[K]^+$, respectively. These ions were also used for quantification by Jeong et al. (2011a), with the exception of potassium. It should be noted that isobaric interferences due to $[AlO]^+$ and $[C_3H_3]^+$ are possible for m/z 43 and 39, respectively (Snyder et al., 2009). However, aluminium-rich particles were not identified in the Paris dataset, and the relative sensitivity of the ATOFMS for potassium relative to organic carbon at m/z 39 is sufficiently high that the isobaric interference did not preclude quantification of the former in this case. Quantification of sodium and chloride was also explored, but the agreement observed with the concurrent measurements was poor. The average contribution of sodium and chloride to the measured $PM_{2.5}$ mass concentration was relatively low (∼ 2 %, as determined by the PILS-IC), and therefore these species were omitted from the quantification procedure. Thus, for the mass reconstruction calculations, it is assumed that all particles are composed entirely of OA, EC, potassium, ammonium, sulphate and nitrate. These species have been demonstrated to account for more than 90 % of annual average $PM_{2.5}$ mass concentrations in Paris (Bressi et al., 2012). Single particle composition was also assumed to be homogeneous for all single particles within each class.

ACPD
13, 10345–10393, 2013

The ATOFMS relative peak area (RPA), defined here as the peak area of each m/z divided by the total dual ion mass spectral peak area, for the marker ions in the number-weighted average mass spectrum were compared directly to the average mass concentrations of each chemical species determined by concurrent OCEC field instrument, HR-ToF-AMS and PILS-IC measurements. RPA was chosen for quantification because it is less sensitive to the variability in ion intensity associated with particle-laser interactions when compared to absolute peak area (Gross et al., 2000). Comparison between the ATOFMS RPA values and mass concentration data from the other instruments enabled the determination of arbitrary relative sensitivity factors (RSFs) for each species. The ATOFMS is subject to different sensitivities for chemical species due to differences in their ionization energies. For example, laboratory studies have previously demonstrated that the ATOFMS RSFs for ammonium and sodium differ by two orders of magnitude (Gross et al., 2000). Matrix effects associated with different internal mixing states may also significantly influence the relative sensitivities observed (Reilly et al., 2000; Reinard and Johnston, 2008; Pratt and Prather, 2009).

The RPA of each species was subsequently calculated for the average mass spectrum of each of the ten carbonaceous particle classes individually. The mass fraction ($\mathrm{mf}_{i,j}$) of each chemical species (i) present in each ATOFMS class (j), was then calculated as follows:

$$\mathrm{mf}_{i,j} = \frac{(\mathrm{RPA}_{i,j} \times \mathrm{RSF}_i)}{\sum_i (\mathrm{RPA}_{i,j} \times \mathrm{RSF}_i)} \quad (1)$$

where $\mathrm{RPA}_{i,j}$ is the relative peak area of each chemical species (i) present in the average mass spectrum of ATOFMS class (j) and RSF_i is the relative sensitivity factor for species (i) determined using the number-weighted average mass spectrum of all 1.50 million carbonaceous particles. The total mass concentration (m_i) of each chemical species was then calculated for each hour of the campaign as follows:

$$m_i = \sum_j (\mathrm{mf}_{i,j} \times m_j) \quad (2)$$

ACPD
13, 10345–10393, 2013

where m_j is the mass concentration of ATOFMS class (j). Finally, the ATOFMS-derived total mass concentrations for each species were multiplied by a factor of 1.24 to account for the low bias of the ATOFMS (inverse of 0.81, Fig. S1). Comparisons of ATOFMS-derived mass concentrations with concurrent measurements for each chemical species are discussed in Sect. 3.2.

A sensitivity analysis was also explored using seven day subsets of the ATOFMS dataset to investigate whether the same quantification approach would enable prediction of the temporality of each chemical species for the remainder of the measurement period. No significant decrease in correlations were observed between the ATOFMS-derived mass concentrations and the other instruments when using these smaller subsets in place of the full ATOFMS dataset, although the slopes do vary significantly, as discussed in detail in the Supplement (Table S1).

Another quantification procedure was also explored using a mass-weighted average mass spectrum generated from the ten carbonaceous classes instead of a number-weighted average, because this was expected to provide a more accurate relative mass contribution for each class. Surprisingly, the resulting reconstructed mass concentrations were almost identical to those obtained using the number-weighted average mass spectrum, due to the similarity between the relative unscaled average number concentrations for each particle class and the relative scaled mass contributions for each particle class (Fig. S3, Table S2). This effect is discussed in the Supplement. The number-weighted average mass spectrum (Fig. S2) was used to generate the reconstructed mass concentrations reported in Sect. 3.2.

2.3 Meteorological analysis

The meteorological analysis used to separate the campaign into periods influenced by air masses of different origin has been described previously (Healy et al., 2012). Marine air masses dominated from 15 January 2010 00:00 [UTC] to 25 January 2010 12:00 and from 28 January 2010 00:00 to 7 February 2010 00:00. Continental air masses prevailed from 25 January 2010 12:00 to 28 January 2010 00:00 and from 7 February

ACPD
13, 10345–10393, 2013

2010 00:00 to 11 February 2010 18:00. A fog event was observed on 18 January 2010, persisting for several hours, and a period of regional stagnation was observed on 23–24 January 2010. It is important to note that marine air masses do not necessarily represent pristine background conditions. Emissions between the Atlantic coast of France and Paris have been demonstrated to affect air quality in the city under low wind speed conditions (Freutel et al., 2013). Thus, during "marine" periods, air quality is expected to be controlled mostly by local and regional scale emissions within France, while during "continental" periods, transboundary emissions from Northwestern and Eastern Europe can also contribute significantly.

2.4 Potential source contribution function

Geographical source regions that might contribute to poor air quality events in Paris were investigated using the potential source contribution function (PSCF). This approach involves combining temporal trends for the variables of interest, ATOFMS particle classes in this case, with archived air mass back trajectories. Seventy two hour air mass back trajectories were generated using the HYbrid Single Particle Lagrangian Integrated Trajectory (HYSPLIT) model (Draxler and Rolph, 2003), run using global data assimilation system (GDAS) data at 1 degree latitude-longitude resolution. Back trajectories were generated for every three hours of the measurement period, and started at 500 m a.g.l.. PSCF is defined as follows:

$$\mathrm{PSCF}_{i,j} = \frac{m_{i,j}}{n_{i,j}} \tag{3}$$

where $n_{i,j}$ is the number of times a trajectory passed through cell (i,j) and $m_{i,j}$ is the number of times a user-defined threshold value was exceeded when a trajectory passed through that cell. The threshold value was set to the 50th percentile of the reconstructed mass concentration for the entire measurement period. A weight function $[W(n_{i,j})]$ was also applied to downweight the contribution of cells that contained less

ACPD
13, 10345–10393, 2013

than three times the average number of points per cell (PPC) (Jeong et al., 2011b) as follows:

$$W(n_{i,j}) = \begin{cases} 0.7 \text{ if } \text{PPC} < n_{i,j} \leq (3 \times \text{PPC}) \\ 0.4 \text{ if } (0.5 \times \text{PPC}) < n_{i,j} \leq \text{PPC} \\ 0.2 \text{ if } n_{i,j} \leq (0.5 \times \text{PPC}) \end{cases} \quad (4)$$

3 Results and discussion

3.1 Carbonaceous ATOFMS classes

Ten carbonaceous single particle classes were identified and quantified using the ATOFMS scaling procedure. Four of these classes belonged to an EC-rich family and have been discussed in detail previously (Healy et al., 2012), but their average mass spectra are also included in the Supplement for clarity (Fig. S4). Briefly, K-EC particles were apportioned to local domestic woodburning and EC-OA particles were apportioned to local vehicle exhaust. These two classes exhibited strong diurnal trends reflecting local activities. The mass-size mode for K-EC particles was larger than that observed for EC-OA particles, a phenomenon that has also been previously observed for biomass burning and fossil fuel BC using SP2 instruments (Schwarz et al., 2008; Laborde et al., 2012). EC-OA-SO_x particles were tentatively identified as local EC-OA particles that had accumulated sulphate, and the highest concentrations for this class were observed during a low wind speed fog event. EC-OA-NO_x particles were tentatively identified as EC-OA particles that had accumulated ammonium nitrate and secondary organic aerosol (SOA), but exhibited a much larger mass-size mode to the other three classes and were associated predominantly with continental transport events.

Average mass spectra and number-size distributions for the six carbonaceous classes that were not reported in Healy et al. (2012) are given in Figs. 1 and 2,

ACPD
13, 10345–10393, 2013

respectively. Three of these classes are characterised by intense signals for potassium and are apportioned to biomass burning, and three are characterised by low signals for potassium and are thus associated with either fossil fuel combustion or SOA formation. All six classes differ significantly in their relative secondary inorganic ion content. Diurnal and temporal trends for each class are provided in Figs. 3 and 4, respectively.

3.1.1 K-OA

K-OA particles exhibited a strong diurnal trend, with higher mass concentrations consistently observed in the evening, as shown in Fig. 3. Similar diurnal behaviour was previously observed for the K-EC class (Healy et al., 2012). An intense base peak for potassium $[K]^+$ dominates the positive ion mass spectrum for K-OA particles while a strong signal is also observed for organic nitrogen in the negative ion mode $[CN]^-$ (Fig. 1). The relative intensities for internally mixed nitrate $[NO_3]^-$ and sulphate $[HSO_4]^-$ are lower than those observed for the other OA classes. The strong diurnal behaviour and relatively small number size mode (280 nm) suggests that these particles are fresh (Figs. 2 and 3), while the relatively high potassium content indicates that local biomass burning represents the most likely source (Silva et al., 1999; Bente et al., 2008; Healy et al., 2010; McGuire et al., 2011; Harrison et al., 2012a; Pagels et al., 2013). Similar diurnal behaviour was observed for the primary BBOA PMF factor apportioned to local domestic biomass burning derived from the HR-ToF-AMS data at the same site (Crippa et al., 2013a), and comparisons are discussed below. There is no obvious dependence upon air mass origin for this class, as expected for a diffuse local source (Fig. 4).

3.1.2 K-OA-NO_x

K-OA-NO_x particles exhibit similar positive ion mass spectra to K-OA particles, but with an additional peak corresponding to ammonium $[NH_4]^+$, and much higher relative peak intensity for nitrate $[NO_3]^-$ in the negative ion mode (Fig. 1). The number-size mode of this class is larger than fresh K-OA particles (310 nm), indicating that K-OA-NO_x

ACPD
13, 10345–10393, 2013

may represent aged biomass burning particles that have accumulated nitrate during transport (Fig. 2). Similar particles have been detected in Cork City, Ireland, a location dominated by primary local emissions, but were observed exclusively under low wind speed conditions, when local processing was favourable (Healy et al., 2010). In that case, a strong diurnal trend was observed, consistent with condensation of ammonium nitrate on local biomass burning particles. The smooth diurnal trend observed for Paris (Fig. 3) supports the importance of regional contributions of aged biomass burning organic aerosol and nitrate (Crippa et al., 2013a). The highest concentrations for this particle class were observed during a regional stagnation event on 23–24 January 2010 (Fig. 4).

3.1.3 K-OA-SO_x

The average K-OA-SO_x mass spectrum is similar to that observed for K-OA-NO_x but with higher signals for ammonium and sulphate. The number-size mode for this class is also similar, albeit slightly larger (325 nm). This class may thus represent aged biomass burning particles that have accumulated ammonium nitrate and sulphate, and potentially SOA during transport. In contrast to K-OA-NO_x particles, the highest concentrations for K-OA-SO_x particles are observed during continental transport events, for example on the 26–27 January 2010 (Fig. 4). Elevated sulphate concentrations in Paris have previously been associated with advection of emissions from Eastern and Northwestern Europe (Bressi et al., 2012). Interestingly however, elevated concentrations ($> 5\,\mu g\,m^{-3}$) of K-OA-SO_x particles are also observed during a low wind speed fog event on 18 January 2010 (Fig. 4). The latter observation indicates that oxidation of SO_2 to form particle phase sulphate can occur on biomass burning particles at a local scale in Paris under low wind speed and high relative humidity conditions.

ACPD
13, 10345–10393, 2013

3.1.4 OA-NO_x

OA-NO_x particles do not exhibit a strong signal for potassium and are characterised instead by a positive ion base peak at m/z 36 $[C_3]^+$, suggesting that these particles do not originate from biomass combustion, but are instead associated either with fossil fuel combustion or SOA formation. Negative ion mass spectra are dominated by nitrate $[NO_3]^-$ (Fig. 1), and this class exhibits a similar temporal trend to that observed for K-OA-NO_x (Fig. 4), suggesting regional scale contributions. Similar particles have been observed in several urban locations and are typically identified as SOA or aged organic aerosol internally mixed with nitrate (Moffet et al., 2008; Qin et al., 2012). These particles are characterised by a broad size distribution with a relatively large number-size mode at 420 nm (Fig. 2), and do not exhibit an obvious diurnal trend (Fig. 3).

3.1.5 OA-SO_x

This class is characterised by mass spectra that are quite similar to OA-NO_x, but with lower signals for nitrate $[NO_3]^-$ and higher signals for sulphate $[HSO_4]^-$. These particles are much smaller (255 nm) than OA-NO_x particles, and have a significant contribution during the local fog event on 18 January 2010, similar to that observed for K-OA-SO_x particles (Fig. 4). The diurnal trend is quite smooth (Fig. 3), and elevated concentrations are observed during periods influenced by continental air masses. Similar particles are routinely observed in ATOFMS field studies, and assigned as SOA or aged organic aerosol that has become internally mixed with sulphate through atmospheric processing (Moffet et al., 2008; Cahill et al., 2012; Qin et al., 2012). It is not possible to determine whether the OA-NO_x and OA-SO_x particle classes represent SOA that has condensed on pre-existing inorganic particles during transport or SOA that has accumulated inorganic ions during transport.

ACPD
13, 10345–10393, 2013

3.1.6 OA-TMA

This particle class is unique in that it is observed exclusively during continental transport events (Fig. 4). The dual ion mass spectra for OA-TMA particles are similar to those observed for OA-SO_x but with an additional intense peak at m/z 59 $[N(CH_3)_3]^+$ corresponding to trimethylamine (TMA) (Fig. 1). This species has been previously identified in single particles detected in Riverside, CA and Toronto, ON (Angelino et al., 2001; Rehbein et al., 2011; McGuire et al., 2011). In the latter case, elevated levels of internally mixed TMA were observed only when relative humidity was high (> 90 %) and air masses arriving at the receptor site had passed over agricultural areas associated with intensive animal husbandry activities. In the case of this work, OA-TMA particles were not observed during a local fog event on 18 January 2010, indicating that local sources of TMA in Paris were negligible (Fig. 4). OA-TMA particles were instead observed during continental transport events characterised by comparatively lower average relative humidity (76 %). These particles are tentatively assigned as internal mixtures of SOA, ammonium nitrate and sulfate that have undergone heterogeneous reaction with gas phase TMA during transport over agricultural areas before arrival in Paris. The absence of concurrent measurements of particulate phase TMA mass concentrations precluded the quantification of this species using ATOFMS data. The relatively large number-size mode for this class (435 nm) (Fig. 2), and the air mass retroplumes for the corresponding continental transport periods (Healy et al., 2012), both suggest that these particles are significantly aged. Potential source regions for transported particles are discussed in Sect. 3.4.

3.2 ATOFMS quantification

The mass fraction of each chemical species calculated for all ten ATOFMS classes was summed to estimate total hourly mass concentrations. The ATOFMS-derived mass concentrations for OA, EC and inorganic ions are compared with data from the HR-ToF-AMS, PILS and Sunset OCEC analyzer in Figs. 5 and 6. The agreement is good in

ACPD
13, 10345–10393, 2013

all cases (R^2 = 0.67–0.78), considering the necessary scaling procedures and the assumption of uniform density and detection efficiency for all particle classes. EC and OA are slightly overestimated by the ATOFMS (slope = 1.14 and 1.16, respectively), while the inorganic ions are underestimated relative to the other instruments (slope = 0.66–0.82). The agreement observed for ammonium, nitrate and sulphate is similar to that obtained by Jeong et al. (2011a) (R^2 = 0.62–0.79). Although effective mass reconstruction was observed for the inorganic ions by Jeong et al. (2011a), the agreement was less satisfactory for EC and OA (R^2 = 0.19 and 0.46, respectively). The improved agreement observed in this work, (R^2 = 0.72 and 0.75, respectively), may be due in part to the greater prevalence of EC in Paris and the inclusion of multiple marker ions for EC and OA (Spencer and Prather, 2006; Pagels et al., 2013).

The average ATOFMS-derived size-resolved mass concentrations for each species are also compared with size-resolved mass concentrations from the HR-ToF-AMS in Fig. S5. The distributions are broadly similar for both instruments, with mass-size modes agreeing within 10 % for the inorganic ions and within 20 % for OA. The size-resolved chemical composition of the reconstructed ATOFMS mass is shown in Fig. 7. At the lowest size detected (150 nm), EC represents approximately 50 % of the total mass, and although the EC mass-size distribution is bimodal (Fig. S5), its mass contribution above 400 nm is very low relative to OA and the inorganic ions. The bimodal mass-size distribution for EC is similar to that previously reported by Healy et al. (2012). At sizes larger than 400 nm the bulk composition is relatively homogeneous, and is dominated by OA and nitrate, in agreement with Crippa et al. (2013a).

The relative mass contribution of each chemical species to each ATOFMS class is shown in Fig. 8 and Table 1. The four EC classes previously described in Healy et al. (2012) are also included. An alternative simpler approach for estimating EC mass concentrations using ATOFMS data was explored by Healy et al. (2012), where these four classes were assumed to be composed entirely of EC for the purpose of simple mass reconstruction. The comparison with thermal/optical EC data was reasonable in that case (R^2 = 0.61), but is improved here (R^2 = 0.72). As demonstrated in Fig. 8,

ACPD
13, 10345–10393, 2013

these 4 classes are not composed entirely of EC, but are internally mixed to differing extents with inorganic ions and OA. The inclusion of EC content from the additional six classes, and the removal of non-EC mass from the four classes reported in Healy et al. (2012), explains the improved agreement.

EC-OA particles associated with fresh local traffic emissions are estimated to be composed of 62 % EC, with an OA/EC ratio of 0.48. EC-OA-SO_x particles, assigned as locally aged vehicle exhaust particles, contain more OA and exhibit an OA/EC ratio of 1.72. When these classes are combined, their total OA/EC ratio is 0.61, a value identical to that determined for the ratio of traffic-related hydrocarbon-like OA (HOA) to traffic-related BC by Crippa et al. (2013a) for the same site and measurement period (0.61). HOA/BC ratios determined for ambient vehicle exhaust particles at a near-road site in New York, NY were estimated to be approximately 1 using a soot particle aerosol mass spectrometer, with lower ratios observed for heavy duty vehicle plumes ($\sim$ 0.7) (Massoli et al., 2012). The majority of HOA (80 %) was found to be internally mixed with BC in that case, in agreement with the ATOFMS results reported here. The relationship between HOA and the two ATOFMS particle classes is discussed further in Sect. 3.3.

K-EC particles associated with local biomass burning are estimated to be composed of 57 % EC. In contrast, K-OA particles are estimated to be comprised of only 14 % EC, but exhibit very similar temporal behaviour to K-EC particles (R^2 = 0.76). These two classes are characterised by very different OA/EC ratios (0.42 and 3.83 for K-EC and K-OA, respectively). This difference in OA/EC ratio is not due to chemical processing, because the relative mass contributions of K-EC and K-OA particles do not exhibit a dependence upon time of day. Both classes are therefore identified as relatively fresh particles associated with local biomass combustion. The ratio of primary OA to EC emitted from domestic wood burners has been demonstrated to be highly variable, and depends upon the appliance chosen and the burning phase (Heringa et al., 2011; Heringa et al., 2012; Pagels et al., 2013). Thus, the observation of more than one chemical mixing state for ambient fresh domestic wood burning particles is logical. Variable hygroscopic growth factors were also observed for particles associated

ACPD
13, 10345–10393, 2013

with local biomass burning emissions for the same measurement period at a separate site in Paris, consistent with the presence of more than one mixing state (Laborde et al., 2012). When the two local ATOFMS biomass burning classes are combined the total OA/EC ratio is determined to be 2.12, a value lower than the local biomass burning OA/BC ratio determined by Crippa et al. (2013a) (3.62). This discrepancy may arise from differences in the apportionment of local and aged biomass burning aerosol contributions using the ATOFMS and HR-ToF-AMS, discussed in the next section.

The EC content of the remaining ATOFMS carbonaceous classes is quite low (Fig. 8). These classes are instead characterised by much higher secondary inorganic ion content, and are also expected to contain significant SOA. It is not possible to separate the relative contributions of aged primary fossil fuel combustion OA and SOA using the methodology described here. Furthermore, it should be noted that although all ten carbonaceous particle classes are estimated to contain at least some EC using this approach, it is unrealistic that all carbonaceous particles should contain a primary EC core. SP2 measurements taken at a separate site for the same period determined that 95 % of particles associated with continental transport did not contain a detectable BC core (Laborde et al., 2012). It is possible that a fraction of the mass apportioned to EC using the ATOFMS quantification approach may arise from fragmentation of organic molecular ions to form $[C_n]^+$ and $[C_n]^-$ fragment ions in the mass spectrometer. Thus some OA would be erroneously detected as EC. The mixing state of SOA is discussed further in the next section.

3.3 Comparison of ATOFMS and HR-ToF-AMS organic aerosol apportionment

The agreement between the ATOFMS reconstructed OA mass concentration and the OA mass concentration detected by the HR-ToF-AMS (R^2 = 0.75, slope = 1.16) provided the opportunity to compare OA source apportionment using both instruments. Positive matrix factorization (PMF) (Ulbrich et al., 2009) of the AMS OA dataset has been described in detail previously by Crippa et al. (2013a). Briefly, five factors were obtained for the LHVP site, corresponding to hydrocarbon-like organic aerosol (HOA),

ACPD
13, 10345–10393, 2013

cooking organic aerosol (COA), biomass burning organic aerosol (BBOA), oxidized organic aerosol (OOA) and less oxidized organic aerosol tentatively assigned as aged biomass burning aerosol (OOA_2-BBOA). By examining the agreement between the ATOFMS OA mass fractions of the single particles classes and the PMF OA factors from the HR-ToF-AMS, the distribution of PMF OA factors across the different single particle mixing states was explored. To the best of the authors' knowledge, this is the first time this comparison has been attempted.

In most cases, the OA content from more than one ATOFMS class was required to achieve reasonable agreement with the HR-ToF-AMS PMF OA factors (Fig. 9). This is not unexpected considering that there are more single particle classes than OA PMF factors. For example, better agreement was observed when HOA was compared with the summed mass concentration of OA contained in the EC-OA and EC-OA-SO_x ATOFMS classes (R^2 = 0.67, slope = 0.40), than when the OA content of the EC-OA class alone was considered (R^2 = 0.57, slope = 0.27). The improved agreement suggests that HOA is distributed across two particle mixing states, one representing fresh vehicle exhaust particles (EC-OA), and one representing more aged vehicle exhaust particles that have accumulated sulphate through local processing (EC-OA-SO_x). However, the ATOFMS mass concentrations are biased low relative to the HR-ToF-AMS HOA mass concentrations. This may be partly due to the lower sizing limit of the ATOFMS (150 nm), although differences in OA apportionment between the two approaches are also expected to contribute to the underestimation.

HR-ToF-AMS BBOA mass concentrations also agreed reasonably well with the summed OA content of the primary ATOFMS K-EC and K-OA particle classes, although the ATOFMS values are again lower (R^2 = 0.56, slope = 0.63). Furthermore, the tentative assignment of the OOA_2-BBOA factor as aged biomass burning aerosol by Crippa et al. (2013a) could be further supported using the ATOFMS dataset. This factor agreed reasonably with the OA content of the aged biomass burning ATOFMS K-OA-NO_x particle class (R^2 = 0.47). K-OA-NO_x particles are significantly internally mixed with nitrate (Fig. 8) and do not exhibit a strong diurnal trend, suggesting a regional contribution.

ACPD
13, 10345–10393, 2013

The highest concentrations are observed during a regional stagnation event on the 23–24 January 2010 (Fig. 4). It is important to note that the ATOFMS clustering and HR-ToF-AMS PMF procedures differ in their separation of fresh and aged aerosol. The former separates single particle types based on their relative carbonaceous and inorganic ion content, while the latter resolves factors based on the temporal variation of the OA mass spectral ions. Thus K-OA and K-OA-NO_x are separated based on differences in nitrate ion intensity (Fig. 1), while BBOA and OOA_2-BBOA are separated based on differences in their temporality and extent of oxidation. The "cut-off" between fresh and aged biomass burning aerosol to produce discrete variables will therefore be different in each case. When the summed OA content of the total fresh and aged ATOFMS biomass burning classes (K-EC, K-OA, K-OA-NO_x) and the sum of the HR-ToF-AMS BBOA and OOA_2-BBOA factors are compared, the agreement improves significantly (R^2 = 0.60, slope = 0.85), highlighting the arbitrary cut-off effect (Fig. S6). This effect may also contribute to the discrepancy between the OA/EC and OA/BC ratios observed for local biomass combustion particles determined using the ATOFMS/HR-ToF-AMS and aethalometer/HR-ToF-AMS approaches, respectively (Crippa et al., 2013a).

The HR-ToF-AMS OOA factor detected in Paris has been previously identified as SOA (Crippa et al., 2013a). Very good agreement was observed between the OOA factor and the sum of the OA content of the remaining five ATOFMS carbonaceous classes (R^2 = 0.81). Each of these ATOFMS classes are characterised by relatively high ammonium, nitrate and sulphate content and are associated with regional/continental scale transport (K-OA-SO_x, OA-SO_x, OA-NO_x, OA-TMA, EC-OA-NO_x). Thus, these aged particles are expected to contain significant SOA. The mixing state of SOA in Paris can therefore be inferred to be relatively heterogeneous, and distributed among five different particle classes during the measurement period. Significantly, no externally mixed SOA was observed. This indicates that either SOA condenses on pre-existing inorganic ion particles, or accumulation of inorganic ions occurs on SOA particles, during transport to Paris. Simultaneous hygroscopic growth factor measurements of continental particles at a separate site also indicate significant secondary inorganic ion and/or

ACPD
13, 10345–10393, 2013

OOA content (GF ≈ 1.6 for dry mobility diameter = 265 nm) (Laborde et al., 2012). The ATOFMS does consistently overestimate the OOA concentration (slope = 1.47), and this may be due in part to the overestimation of the ATOFMS total OA relative to the HR-ToF-AMS total OA (Fig. 6). However, HOA mass concentrations and BBOA are simultaneously underestimated by the ATOFMS (Fig. 9), indicating that differences in apportionment between the two approaches may also contribute to the bias.

Notably, none of the ATOFMS classes correlated well with cooking organic aerosol (COA), which was estimated to have a contribution of 17 % to total OA mass at the LHVP site (Crippa et al., 2013a). Combinations of the OA mass fractions of the different ATOFMS particle classes did not correlate well with COA either. Thus it appears that the ATOFMS does not detect primary OA associated with urban cooking activities efficiently. It is possible that cooking aerosol is too small to be detected in the size range investigated here, with previous studies determining number-size modes below 100 nm for primary cooking particles (Wallace et al., 2004; Wallace, 2006; Ogulei et al., 2006; Evans et al., 2008). Another possibility is that cooking particles are sized correctly but not desorbed/ionized efficiently by the UV laser. Charbroiling and oil frying aerosol has been previously determined to contain saturated alkanes, alkenes, cycloalkanes, fatty acids, and no detectable EC (Schauer et al., 1999; Mohr et al., 2009; Allan et al., 2010). Low EC content, and potentially low polycyclic aromatic hydrocarbon content, for cooking aerosol relative to the other carbonaceous particle mixing states could result in low absorption efficiency at 266 nm, and may explain its absence in the ATOFMS mass spectral dataset. Investigation of the ratio of particles successfully and unsuccessfully ionized by the ATOFMS (hit/miss ratio) did not uncover a trend that correlated with COA either. Therefore it could not be determined whether cooking particles were below the size range investigated or were not ionized efficiently in this study. A cooking-related particle class also remained undetected by ATOFMS in recent studies focused on OA source apportionment in London, England and Cork, Ireland, while COA mass concentrations $> 2\,\mu g\,m^3$ were simultaneously detected by co-located AMS instruments (Dall'Osto and Harrison, 2012; Dall'Osto et al., 2012).

ACPD
13, 10345–10393, 2013

3.4 Local and regional/continental scale source apportionment

The relative mass contributions of the ten carbonaceous particle classes to each chemical species, and to total mass in the size range investigated (150–1067 nm, d_{va}), were also calculated as shown in Fig. S7 and Table S3. By examining chemical composition and temporality, each class was associated either with local activities or regional/continental scale transport. "Local" classes were defined as those that exhibited a strong diurnal trend and/or contained OA mass fractions that correlated well with the primary HR-ToF-AMS HOA or BBOA factors (K-EC, K-OA, EC-OA, EC-OA-SO_x,). "Transported" classes were defined as those with no obvious diurnal trend and high secondary inorganic ion content (K-OA-NO_x, KOA-SO_x, OA-NO_x, OA-SO_x, OA-TMA, EC-OA-NO_x). Although this classification procedure has inherent limitations, for example elevated concentrations of OA-SO_x and K-OA-SO_x particles are also observed during a local fog processing event on 18 January 2010, the approach enables an estimation of the relative impact of transported emissions upon local air quality in Paris.

Temporal trends, average chemical composition and wind dependence for local and transported particles are shown in Figs. 10 and 11. Local particles persist throughout the entire measurement period, are characterized by low inorganic ion content (< 25 %), and exhibit little dependence upon wind direction. Transported particles are characterized by much higher inorganic ion content (62 %), and much lower concentrations are observed during periods influenced by fast-moving marine air masses (28 January 2010–7 February 2010). These particles also exhibit a comparatively strong dependence upon northeasterly wind direction and the highest mass concentrations are observed during two continental transport events (26–27 January 2010 and 11 February 2010). PSCF was used to identify potential source regions for transported particles arriving in Paris. As shown in Fig. S8, local particles are observed at elevated mass concentrations independent of whether air masses originate over the Atlantic Ocean or continental Europe. Conversely, transported particles are observed at elevated concentrations almost exclusively when air masses pass through Northwestern

ACPD
13, 10345–10393, 2013

and Eastern Europe before arriving in Paris. The results indicate that particulate matter containing significant internally mixed SOA and inorganic ion content detected in Paris is associated predominantly with transboundary emissions originating outside France.

As shown in Fig. 12, the majority of EC (59 %) is attributed to local emissions from vehicular traffic and domestic biomass burning. This estimate for the local contribution to EC is lower than that previously reported by Healy et al. (2012) (79 %). This difference can be explained by the different approaches used. Here, the EC mass fractions of the local primary ATOFMS carbonaceous classes are considered, while Healy et al. (2012) employed a size limit of 400 nm to separate local (< 400 nm) and transported (> 400 nm) EC contributions. Thus, the majority of EC is attributed to local sources irrespective of the approach used, but there is better agreement between the Sunset EC data and the reconstructed ATOFMS EC mass concentrations determined in this study, as discussed in Sect. 3.2.

EC is the only species for which local emissions are estimated to have the highest contribution. In contrast, the majority of OA, ammonium, sulphate and nitrate are associated with regional/continental scale emissions (Fig. 12). Only 24, 5, 16 and 8 % of OA, ammonium, sulphate and nitrate are associated with fresh local emissions in Paris, respectively. The relative contributions of local and transported emissions to the total ATOFMS-derived PM mass concentration are estimated to be 22 and 78 %, respectively. These observations are consistent with previous studies involving multiple sampling sites in and around Paris. Bressi et al. (2012) demonstrated that annual average $PM_{2.5}$ mass concentrations measured at an urban site in Paris were only 26 % higher than those measured at a rural site 50 km to the northwest of the city. Secondary inorganic ion and SOA mass concentrations in Paris have also been associated predominantly with regional and/or continental scale emissions, with minimal input from local activities in several recent studies (Sciare et al., 2010; Sciare et al., 2011; Bressi et al., 2012; Crippa et al., 2013a).

ACPD
13, 10345–10393, 2013

4 Conclusions

Single particle mass spectra have been used to estimate the quantitative chemical mixing state of carbonaceous particles in Paris, France as part of the MEGAPOLI winter campaign (2010). Good agreement (R^2 = 0.67–0.78) was observed between ATOFMS-derived mass concentrations for EC, OA, potassium, ammonium, sulphate and nitrate, and those measured using simultaneous HR-ToF-AMS, thermal optical OCEC analyser and PILS-IC instruments. The results indicate that quantitative mixing state information for multiple chemical species can be estimated simultaneously using this approach. Ten discrete mixing states were identified for carbonaceous particles, differing in their relative EC, OA and inorganic ion content. The distribution of OA across the different single particle mixing states was compared with HR-ToF-AMS OA PMF factors, and good agreement was observed (R^2 = 0.47–0.81). Two chemically distinct mixing states were identified for EC-rich particles associated with vehicle exhaust. One was associated with fresh emissions, while the other was characterised by higher sulphate content and associated with locally processed vehicle exhaust. The sum of the OA content of these particle classes agreed well with the HR-ToF-AMS HOA factor (R^2 = 0.67). Two mixing states were also identified for locally emitted biomass combustion particles, one dominated by EC, the other dominated by OA, with different OA/EC ratios associated with different combustion conditions. Aged biomass burning particles, significantly internally mixed with nitrate, were found to persist throughout the measurement period, supporting the identification of the HR-ToF-AMS OOA_2-BBOA PMF factor by Crippa et al. (2013a). The sum of the ATOFMS OA content for fresh and aged biomass burning particles agreed well with the sum of the HR-ToF-AMS BBOA and OOA_2-BBOA factors (R^2 = 0.60). Finally, the OA content of five ATOFMS aged carbonaceous particle classes, significantly internally mixed to differing extents with ammonium, nitrate and sulphate, also agreed very well with the HR-ToF-AMS OOA factor (R^2 = 0.81), highlighting the complexity of the mixing state of SOA in Paris.

ACPD
13, 10345–10393, 2013

Based on temporality and chemical mixing state, the ten carbonaceous classes were assigned either to local or transported emissions. Although the majority of EC (59 %) is estimated to be emitted locally, the majority of OA, ammonium, sulphate and nitrate are estimated to arise from sources outside the city. Only 22 % of the total ATOFMS-derived particle mass is apportioned to local emissions, with 78 % apportioned to transported emissions. These findings are consistent with recent studies demonstrating the homogeneity of PM mass concentrations and bulk composition in Paris and the surrounding rural areas, and highlight the significant impact of regional and continental scale emissions upon local air quality (Sciare et al., 2010; Bressi et al., 2012; Freutel et al., 2013; Crippa et al., 2013a).

Supplementary material related to this article is available online at: http://www.atmos-chem-phys-discuss.net/13/10345/2013/acpd-13-10345-2013-supplement.pdf.

Acknowledgements. This research has been funded by the Higher Education Authority Ireland under PRTLI cycle IV, the Irish Research Council for Engineering and Technology, the European Union's Seventh Framework Programme FP/2007-2011 (MEGAPOLI) and the Marie Curie Action FP7-PEOPLE-IOF-2011 (Project: CHEMBC, No. 299755). The authors would also like to thank Valerie Gros, Hervé Petetin, Qijie Zhang and Matthias Beekmann for logistical help and useful discussions on regional and continental pollution in Paris. Meteorological data was provided by Météo-France.

References

Allan, J. D., Williams, P. I., Morgan, W. T., Martin, C. L., Flynn, M. J., Lee, J., Nemitz, E., Phillips, G. J., Gallagher, M. W., and Coe, H.: Contributions from transport, solid fuel burning and cooking to primary organic aerosols in two UK cities, Atmos. Chem. Phys., 10, 647–668, doi:10.5194/acp-10-647-2010, 2010.

ACPD
13, 10345–10393, 2013

Allen, J. O., Fergenson, D. P., Gard, E. E., Hughes, L. S., Morrical, B. D., Kleeman, M. J., Gross, D. S., Galli, M. E., Prather, K. A., and Cass, G. R.: Particle detection efficiencies of aerosol time of flight mass spectrometers under ambient sampling conditions, Environ. Sci. Technol., 34, 211–217, doi:10.1021/es9904179, 2000.

Angelino, S., Suess, D. T., and Prather, K. A.: Formation of aerosol particles from reactions of secondary and tertiary alkylamines: characterization by aerosol time-of-flight mass spectrometry, Environ. Sci. Technol., 35, 3130–3138, doi:10.1021/es0015444, 2001.

Ault, A. P., Gaston, C. J., Wang, Y., Dominguez, G., Thiemens, M. H., and Prather, K. A.: Characterization of the single particle mixing state of individual ship plume events measured at the port of Los Angeles, Environ. Sci. Technol., 44, 1954–1961, doi:10.1021/es902985h, 2010.

Bae, M.-S., Schauer, J. J., DeMinter, J. T., Turner, J. R., Smith, D., and Cary, R. A.: Validation of a semi-continuous instrument for elemental carbon and organic carbon using a thermal-optical method, Atmos. Environ., 38, 2885–2893, doi:10.1016/j.atmosenv.2004.02.027, 2004.

Baeza-Romero, M. T., Wilson, J. M., Fitzpatrick, E. M., Jones, J. M., and Williams, A.: In situ study of soot from the combustion of a biomass pyrolysis intermediate–Eugenol–and n-decane using aerosol time of flight mass spectrometry, Energ. Fuel., 24, 439–445, doi:10.1021/ef9008746, 2009.

Bein, K. J., Zhao, Y., Johnston, M. V., and Wexler, A. S.: Identification of sources of atmospheric PM at the Pittsburgh Supersite – Part III: Source characterization, Atmos. Environ., 41, 3974–3992, 2007.

Bente, M., Sklorz, M., Streibel, T., and Zimmermann, R.: Online laser desorption-multiphoton postionization mass spectrometry of individual aerosol particles: molecular source indicators for particles emitted from different traffic-related and wood combustion sources, Anal. Chem., 80, 8991–9004, doi:10.1021/ac801295f, 2008.

Bhave, P. V., Fergenson, D. P., Prather, K. A., and Cass, G. R.: Source apportionment of fine particulate matter by clustering single-particle data: tests of receptor model accuracy, Environ. Sci. Technol., 35, 2060–2072, doi:10.1021/es0017413, 2001.

Birmili, W., Stratmann, F., and Wiedensohler, A.: Design of a DMA-based size spectrometer for a large particle size range and stable operation, J. Aerosol Sci., 30, 549–553, doi:10.1016/s0021-8502(98)00047-0, 1999.

ACPD
13, 10345–10393, 2013

Bressi, M., Sciare, J., Ghersi, V., Bonnaire, N., Nicolas, J. B., Petit, J.-E., Moukhtar, S., Rosso, A., Mihalopoulos, N., and Féron, A.: A one-year comprehensive chemical characterisation of fine aerosol ($PM_{2.5}$) at urban, suburban and rural background sites in the region of Paris (France), Atmos. Chem. Phys. Discuss., 12, 29391–29442, doi:10.5194/acpd-12-29391-2012, 2012.

Cahill, J. F., Suski, K., Seinfeld, J. H., Zaveri, R. A., and Prather, K. A.: The mixing state of carbonaceous aerosol particles in northern and southern California measured during CARES and CalNex 2010, Atmos. Chem. Phys., 12, 10989–11002, doi:10.5194/acp-12-10989-2012, 2012.

Chameides, W. L., Kasibhatla, P. S., Yienger, J., and Levy, H.: Growth of continental-scale metro-agro-plexes, regional ozone pollution, and world food production, Science, 264, 74–77, doi:10.1126/science.264.5155.74, 1994.

Crippa, M., DeCarlo, P. F., Slowik, J. G., Mohr, C., Heringa, M. F., Chirico, R., Poulain, L., Freutel, F., Sciare, J., Cozic, J., Di Marco, C. F., Elsasser, M., Nicolas, J. B., Marchand, N., Abidi, E., Wiedensohler, A., Drewnick, F., Schneider, J., Borrmann, S., Nemitz, E., Zimmermann, R., Jaffrezo, J.-L., Prévôt, A. S. H., and Baltensperger, U.: Wintertime aerosol chemical composition and source apportionment of the organic fraction in the metropolitan area of Paris, Atmos. Chem. Phys., 13, 961-981, doi:10.5194/acp-13-961-2013, 2013a.

Crippa, M., El Haddad, I., Slowik, J. G., DeCarlo, P. F., Mohr, C., Heringa, M. F., Chirico, R., Marchand, N., Sciare, J., Baltensperger, U., and Prévôt, A. S. H.: Identification of marine and continental aerosol sources in Paris using high resolution aerosol mass spectrometry, J. Geophys. Res.-Atmos., doi:10.1029/jgrd.50151, 2013b.

Cross, E. S., Slowik, J. G., Davidovits, P., Allan, J. D., Worsnop, D. R., Jayne, J. T., Lewis, D. K., Canagaratna, M., and Onasch, T. B.: Laboratory and Ambient Particle Density Determinations using Light Scattering in Conjunction with Aerosol Mass Spectrometry, Aerosol Sci. Tech., 41, 343–359, doi:10.1080/02786820701199736, 2007.

Cross, E. S., Onasch, T. B., Canagaratna, M., Jayne, J. T., Kimmel, J., Yu, X.-Y., Alexander, M. L., Worsnop, D. R., and Davidovits, P.: Single particle characterization using a light scattering module coupled to a time-of-flight aerosol mass spectrometer, Atmos. Chem. Phys., 9, 7769–7793, doi:10.5194/acp-9-7769-2009, 2009.

Dall'Osto, M. and Harrison, R. M.: Urban organic aerosols measured by single particle mass spectrometry in the megacity of London, Atmos. Chem. Phys., 12, 4127–4142, doi:10.5194/acp-12-4127-2012, 2012.

ACPD
13, 10345–10393, 2013

Dall'Osto, M., Ovadnevaite, J., Ceburnis, D., Martin, D., Healy, R. M., O'Connor, I. P., Sodeau, J. R., Wenger, J. C., and O'Dowd, C.: Characterization of urban aerosol in Cork City (Ireland) using aerosol mass spectrometry, Atmos. Chem. Phys. Discuss., 12, 29657–29704, doi:10.5194/acpd-12-29657-2012, 2012.

DeCarlo, P. F., Kimmel, J. R., Trimborn, A., Northway, M. J., Jayne, J. T., Aiken, A. C., Gonin, M., Fuhrer, K., Horvath, T., Docherty, K. S., Worsnop, D. R., and Jimenez, J. L.: Field-Deployable, High-Resolution, Time-of-Flight Aerosol Mass Spectrometer, Anal. Chem., 78, 8281–8289, doi:10.1021/ac061249n, 2006.

Draxler, R. R. and Rolph, G. D.: HYSPLIT (Hybrid Single-Particle Lagrangian Integrated Trajectory) model v 4.9: http://www.arl.noaa.gov/ready/hysplit4.html (last access: February 2013), 2003.

Evans, G. J., Peers, A., and Sabaliauskas, K.: Particle dose estimation from frying in residential settings, Indoor Air, 18, 499–510, doi:10.1111/j.1600-0668.2008.00551.x, 2008.

Favez, O., Cachier, H., Sciare, J., Sarda-Estève, R., and Martinon, L.: Evidence for a significant contribution of wood burning aerosols to $PM_{2.5}$ during the winter season in Paris, France, Atmos. Environ., 43, 3640–3644, doi:10.1016/j.atmosenv.2009.04.035, 2009.

Ferge, T., Karg, E., Schröppel, A., Coffee, K. R., Tobias, H. J., Frank, M., Gard, E. E., and Zimmermann, R.: Fast determination of the relative elemental and organic carbon content of aerosol samples by on-line single-particle aerosol time-of-flight mass spectrometry, Environ. Sci. Technol., 40, 3327–3335, doi:10.1021/es050799k, 2006.

Fergenson, D. P., Song, X.-H., Ramadan, Z., Allen, J. O., Hughes, L. S., Cass, G. R., Hopke, P. K., and Prather, K. A.: Quantification of ATOFMS data by multivariate methods, Anal. Chem., 73, 3535–3541, doi:10.1021/ac010022j, 2001.

Freutel, F., Schneider, J., Drewnick, F., von der Weiden-Reinmüller, S.-L., Crippa, M., Prévôt, A. S. H., Baltensperger, U., Poulain, L., Wiedensohler, A., Sciare, J., Sarda-Estève, R., Burkhart, J. F., Eckhardt, S., Stohl, A., Gros, V., Colomb, A., Michoud, V., Doussin, J. F., Borbon, A., Haeffelin, M., Morille, Y., Beekmann, M., and Borrmann, S.: Aerosol particle measurements at three stationary sites in the megacity of Paris during summer 2009: meteorology and air mass origin dominate aerosol particle composition and size distribution, Atmos. Chem. Phys., 13, 933–959, doi:10.5194/acp-13-933-2013, 2013.

Froyd, K. D., Murphy, S. M., Murphy, D. M., de Gouw, J. A., Eddingsaas, N. C., and Wennberg, P. O.: Contribution of isoprene-derived organosulfates to free tropospheric

ACPD
13, 10345–10393, 2013

aerosol mass, P. Natl. Acad. Sci. USA, 107, 21360–21365, doi:10.1073/pnas.1012561107, 2010.
Gao, Y., Liu, X., Zhao, C., and Zhang, M.: Emission controls versus meteorological conditions in determining aerosol concentrations in Beijing during the 2008 Olympic Games, Atmos. Chem. Phys., 11, 12437–12451, doi:10.5194/acp-11-12437-2011, 2011.
Gard, E., Mayer, J. E., Morrical, B. D., Dienes, T., Fergenson, D. P., and Prather, K. A.: Real-time analysis of individual atmospheric aerosol particles: design and performance of a portable ATOFMS, Anal. Chem., 69, 4083–4091, doi:10.1021/ac970540n, 1997.
Gros, V., Gaimoz, C., Herrmann, F., Custer, T., Williams, J., Bonsang, B., Sauvage, S., Locoge, N., d'Argouges, O., Sarda-Estève, R., and Sciare, J.: Volatile organic compounds sources in Paris in spring 2007. Part I: Qualitative analysis, Environ. Chem., 8, 74–90, doi:10.1071/EN10068, 2011.
Gross, D. S., Galli, M. E., Silva, P. J., and Prather, K. A.: Relative sensitivity factors for alkali metal and ammonium cations in single-particle aerosol time-of-flight mass spectra, Anal. Chem., 72, 416–422, 2000.
Gross, D. S., Atlas, R., Rzeszotarski, J., Turetsky, E., Christensen, J., Benzaid, S., Olsen, J., Smith, T., Steinberg, L., Sulman, J., Ritz, A., Anderson, B., Nelson, C., Musicant, D. R., Chen, L., Snyder, D. C., and Schauer, J. J.: Environmental chemistry through intelligent atmospheric data analysis, Environ. Modell. Softw., 25, 760–769, doi:10.1016/j.envsoft.2009.12.001, 2010.
Harrison, R. M., Beddows, D. C. S., Hu, L., and Yin, J.: Comparison of methods for evaluation of wood smoke and estimation of UK ambient concentrations, Atmos. Chem. Phys., 12, 8271–8283, doi:10.5194/acp-12-8271-2012, 2012a.
Harrison, R. M., Dall'Osto, M., Beddows, D. C. S., Thorpe, A. J., Bloss, W. J., Allan, J. D., Coe, H., Dorsey, J. R., Gallagher, M., Martin, C., Whitehead, J., Williams, P. I., Jones, R. L., Langridge, J. M., Benton, A. K., Ball, S. M., Langford, B., Hewitt, C. N., Davison, B., Martin, D., Petersson, K. F., Henshaw, S. J., White, I. R., Shallcross, D. E., Barlow, J. F., Dunbar, T., Davies, F., Nemitz, E., Phillips, G. J., Helfter, C., Di Marco, C. F., and Smith, S.: Atmospheric chemistry and physics in the atmosphere of a developed megacity (London): an overview of the REPARTEE experiment and its conclusions, Atmos. Chem. Phys., 12, 3065–3114, doi:10.5194/acp-12-3065-2012, 2012b.
Heal, M. R., Kumar, P., and Harrison, R. M.: Particles, air quality, policy and health, Chem. Soc. Rev., 41, 6606–6630, 2012.

ACPD
13, 10345–10393, 2013

Healy, R. M., Hellebust, S., Kourtchev, I., Allanic, A., O'Connor, I. P., Bell, J. M., Healy, D. A., Sodeau, J. R., and Wenger, J. C.: Source apportionment of $PM_{2.5}$ in Cork Harbour, Ireland using a combination of single particle mass spectrometry and quantitative semi-continuous measurements, Atmos. Chem. Phys., 10, 9593–9613, doi:10.5194/acp-10-9593-2010, 2010.

Healy, R. M., Sciare, J., Poulain, L., Kamili, K., Merkel, M., Müller, T., Wiedensohler, A., Eckhardt, S., Stohl, A., Sarda-Estève, R., McGillicuddy, E., O'Connor, I. P., Sodeau, J. R., and Wenger, J. C.: Sources and mixing state of size-resolved elemental carbon particles in a European megacity: Paris, Atmos. Chem. Phys., 12, 1681–1700, doi:10.5194/acp-12-1681-2012, 2012.

Heringa, M. F., DeCarlo, P. F., Chirico, R., Tritscher, T., Dommen, J., Weingartner, E., Richter, R., Wehrle, G., Prévôt, A. S. H., and Baltensperger, U.: Investigations of primary and secondary particulate matter of different wood combustion appliances with a high-resolution time-of-flight aerosol mass spectrometer, Atmos. Chem. Phys., 11, 5945–5957, doi:10.5194/acp-11-5945-2011, 2011.

Heringa, M. F., DeCarlo, P. F., Chirico, R., Lauber, A., Doberer, A., Good, J., Nussbaumer, T., Keller, A., Burtscher, H., Richard, A., Miljevic, B., Prevot, A. S. H., and Baltensperger, U.: Time-resolved characterization of primary emissions from residential wood combustion appliances, Environ. Sci. Technol., 46, 11418–11425, doi:10.1021/es301654w, 2012.

Hinz, K.-P., Trimborn, A., Weingartner, E., Henning, S., Baltensperger, U., and Spengler, B.: Aerosol single particle composition at the Jungfraujoch, J. Aerosol Sci., 36, 123–145, doi:10.1016/j.jaerosci.2004.08.001, 2005.

Jeong, C.-H., McGuire, M. L., Godri, K. J., Slowik, J. G., Rehbein, P. J. G., and Evans, G. J.: Quantification of aerosol chemical composition using continuous single particle measurements, Atmos. Chem. Phys., 11, 7027–7044, doi:10.5194/acp-11-7027-2011, 2011a.

Jeong, C. H., McGuire, M. L., Herod, D., Dann, T., Dabek-Zlotorzynska, E., Wang, D., Ding, L., Celo, V., Mathieu, D., and Evans, G. J.: Receptor model based identification of $PM_{2.5}$ sources in Canadian cities, Atmos. Poll. Res., 2, 158–171, 2011b.

Kane, D. B. and Johnston, M. V.: Size and composition biases on the detection of individual ultrafine particles by aerosol mass spectrometry, Environ. Sci. Technol., 34, 4887–4893, doi:10.1021/es001323y, 2000.

Laborde, M., Crippa, M., Tritscher, T., Jurányi, Z., DeCarlo, P. F., Temime-Roussel, B., Marchand, N., Eckhardt, S., Stohl, A., Baltensperger, U., Prévôt, A. S. H., Weingartner, E., and

ACPD
13, 10345–10393, 2013

Gysel, M.: Black carbon physical properties and mixing state in the European megacity Paris, Atmos. Chem. Phys. Discuss., 12, 25121–25180, doi:10.5194/acpd-12-25121-2012, 2012.
Lawrence, M. G., Butler, T. M., Steinkamp, J., Gurjar, B. R., and Lelieveld, J.: Regional pollution potentials of megacities and other major population centers, Atmos. Chem. Phys., 7, 3969–3987, doi:10.5194/acp-7-3969-2007, 2007.
Liu, S., Russell, L. M., Sueper, D. T., and Onasch, T. B.: Organic particle types by single-particle measurements using a time-of-flight aerosol mass spectrometer coupled with a light scattering module, Atmos. Meas. Tech., 6, 187–197, doi:10.5194/amt-6-187-2013, 2013.
Massoli, P., Fortner, E. C., Canagaratna, M. R., Williams, L. R., Zhang, Q., Sun, Y., Schwab, J. J., Trimborn, A., Onasch, T. B., Demerjian, K. L., Kolb, C. E., Worsnop, D. R., and Jayne, J. T.: Pollution gradients and chemical characterization of particulate matter from vehicular traffic near major roadways: results from the 2009 queens college air quality study in NYC, Aerosol Sci. Tech., 46, 1201–1218, doi:10.1080/02786826.2012.701784, 2012.
McGuire, M. L., Jeong, C.-H., Slowik, J. G., Chang, R. Y.-W., Corbin, J. C., Lu, G., Mihele, C., Rehbein, P. J. G., Sills, D. M. L., Abbatt, J. P. D., Brook, J. R., and Evans, G. J.: Elucidating determinants of aerosol composition through particle-type-based receptor modeling, Atmos. Chem. Phys., 11, 8133–8155, doi:10.5194/acp-11-8133-2011, 2011.
Moffet, R. C., de Foy, B., Molina, L. T., Molina, M. J., and Prather, K. A.: Measurement of ambient aerosols in northern Mexico City by single particle mass spectrometry, Atmos. Chem. Phys., 8, 4499–4516, doi:10.5194/acp-8-4499-2008, 2008.
Mohr, C., Huffman, J. A., Cubison, M. J., Aiken, A. C., Docherty, K. S., Kimmel, J. R., Ulbrich, I. M., Hannigan, M., and Jimenez, J. L.: Characterization of primary organic aerosol emissions from meat cooking, trash burning, and motor vehicles with high-resolution aerosol mass spectrometry and comparison with ambient and chamber observations, Environ. Sci. Technol., 43, 2443–2449, doi:10.1021/es8011518, 2009.
Molina, L. T., Madronich, S., Gaffney, J. S., Apel, E., de Foy, B., Fast, J., Ferrare, R., Herndon, S., Jimenez, J. L., Lamb, B., Osornio-Vargas, A. R., Russell, P., Schauer, J. J., Stevens, P. S., Volkamer, R., and Zavala, M.: An overview of the MILAGRO 2006 Campaign: Mexico City emissions and their transport and transformation, Atmos. Chem. Phys., 10, 8697–8760, doi:10.5194/acp-10-8697-2010, 2010.
Molina, M. J. and Molina, L. T.: Megacities and Atmospheric Pollution, J. Air Waste Manage., 54, 644–680, doi:10.1080/10473289.2004.10470936, 2004.

ACPD
13, 10345–10393, 2013

Ogulei, D., Hopke, P. K., and Wallace, L. A.: Analysis of indoor particle size distributions in an occupied townhouse using positive matrix factorization, Indoor Air, 16, 204–215, doi:10.1111/j.1600-0668.2006.00418.x, 2006.

Pagels, J., Dutcher, D. D., Stolzenburg, M. R., McMurry, P. H., Gälli, M. E., and Gross, D. S.: Fine-particle emissions from solid biofuel combustion studied with single-particle mass spectrometry: Identification of markers for organics, soot, and ash components, J. Geophys. Res.-Atmos., doi:10.1029/2012jd018389, 2013.

Peltier, R. E., Weber, R. J., and Sullivan, A. P.: Investigating a liquid-based method for online organic carbon detection in atmospheric particles, Aerosol Sci. Tech., 41, 1117–1127, 2007.

Pratt, K. A. and Prather, K. A.: Real-time, single-particle volatility, size, and chemical composition measurements of aged urban aerosols, Environ. Sci. Technol., 43, 8276–8282, doi:10.1021/es902002t, 2009.

Pratt, K. A. and Prather, K. A.: Mass spectrometry of atmospheric aerosols – recent developments and applications. Part I: Off-line mass spectrometry techniques, Mass Spectrom. Rev., 31, 1–16, doi:10.1002/mas.20322, 2012.

Pratt, K. A., Hatch, L. E., and Prather, K. A.: Seasonal volatility dependence of ambient particle phase amines, Environ. Sci. Technol., 43, 5276–5281, doi:10.1021/es803189n, 2009.

Qin, X., Bhave, P. V., and Prather, K. A.: Comparison of two methods for obtaining quantitative mass concentrations from aerosol time-of-flight mass spectrometry measurements, Anal. Chem., 78, 6169–6178, doi:10.1021/ac060395q, 2006.

Qin, X., Pratt, K. A., Shields, L. G., Toner, S. M., and Prather, K. A.: Seasonal comparisons of single-particle chemical mixing state in Riverside, CA, Atmos. Environ., 59, 587–596, doi:10.1016/j.atmosenv.2012.05.032, 2012.

Rehbein, P. J. G., Jeong, C.-H., McGuire, M. L., Yao, X., Corbin, J. C., and Evans, G. J.: Cloud and fog processing enhanced gas-to-particle partitioning of trimethylamine, Environ. Sci. Technol., 45, 4346–4352, doi:10.1021/es1042113, 2011.

Reilly, P. T. A., Lazar, A. C., Gieray, R. A., Whitten, W. B., and Ramsey, J. M.: The elucidation of charge-transfer-induced matrix effects in environmental aerosols via real-time aerosol mass spectral analysis of individual airborne particles, Aerosol Sci. Tech., 33, 135–152, doi:10.1080/027868200410895, 2000.

Reinard, M. S. and Johnston, M. V.: Ion formation mechanism in laser desorption ionization of individual nanoparticles, J. Am. Soc. Mass Spectr., 19, 389–399, doi:10.1016/j.jasms.2007.11.017, 2008.

ACPD
13, 10345–10393, 2013

Reinard, M. S., Adou, K., Martini, J. M., and Johnston, M. V.: Source characterization and identification by real-time single particle mass spectrometry, Atmos. Environ., 41, 9397–9409, 2007.

Schauer, J. J., Kleeman, M. J., Cass, G. R., and Simoneit, B. R. T.: Measurement of emissions from air pollution sources. 1. C_1 through C_{29} organic compounds from meat charbroiling, Environ. Sci. Technol., 33, 1566–1577, doi:10.1021/es980076j, 1999.

Schwarz, J. P., Gao, R. S., Spackman, J. R., Watts, L. A., Thomson, D. S., Fahey, D. W., Ryerson, T. B., Peischl, J., Holloway, J. S., Trainer, M., Frost, G. J., Baynard, T., Lack, D. A., de Gouw, J. A., Warneke, C., and Del Negro, L. A.: Measurement of the mixing state, mass, and optical size of individual black carbon particles in urban and biomass burning emissions, Geophys. Res. Lett., 35, L13810, doi:10.1029/2008gl033968, 2008.

Sciare, J., d'Argouges, O., Zhang, Q. J., Sarda-Estève, R., Gaimoz, C., Gros, V., Beekmann, M., and Sanchez, O.: Comparison between simulated and observed chemical composition of fine aerosols in Paris (France) during springtime: contribution of regional versus continental emissions, Atmos. Chem. Phys., 10, 11987–12004, doi:10.5194/acp-10-11987-2010, 2010.

Sciare, J., d'Argouges, O., Sarda-Estève, R., Gaimoz, C., Dolgorouky, C., Bonnaire, N., Favez, O., Bonsang, B., and Gros, V.: Large contribution of water-insoluble secondary organic aerosols in the region of Paris (France) during wintertime, J. Geophys. Res., 116, D22203, doi:10.1029/2011jd015756, 2011.

Silva, P. J., Liu, D. Y., Noble, C. A., and Prather, K. A.: Size and chemical characterization of individual particles resulting from biomass burning of local Southern California species, Environ. Sci. Technol., 33, 3068–3076, 1999.

Snyder, D. C., Schauer, J. J., Gross, D. S., and Turner, J. R.: Estimating the contribution of point sources to atmospheric metals using single-particle mass spectrometry, Atmos. Environ., 43, 4033–4042, 2009.

Spencer, M. T. and Prather, K. A.: Using ATOFMS to Determine OC/EC Mass Fractions in Particles, Aerosol Sci. Tech., 40, 585–594, 2006.

Su, Y., Sipin, M. F., Spencer, M. T., Qin, X., Moffet, R. C., Shields, L. G., Prather, K. A., Venkatachari, P., Jeong, C.-H., Kim, E., Hopke, P. K., Gelein, R. M., Utell, M. J., Oberdörster, G., Berntsen, J., Devlin, R. B., and Chen, L. C.: Real-time characterization of the composition of individual particles emitted from ultrafine particle concentrators, Aerosol Sci. Tech., 40, 437–455, doi:10.1080/02786820600660887, 2006.

ACPD
13, 10345–10393, 2013

Tuch, T. M., Haudek, A., Müller, T., Nowak, A., Wex, H., and Wiedensohler, A.: Design and performance of an automatic regenerating adsorption aerosol dryer for continuous operation at monitoring sites, Atmos. Meas. Tech., 2, 417–422, doi:10.5194/amt-2-417-2009, 2009.

Ulbrich, I. M., Canagaratna, M. R., Zhang, Q., Worsnop, D. R., and Jimenez, J. L.: Interpretation of organic components from Positive Matrix Factorization of aerosol mass spectrometric data, Atmos. Chem. Phys., 9, 2891–2918, doi:10.5194/acp-9-2891-2009, 2009.

Wallace, L.: Indoor sources of ultrafine and accumulation mode particles: size distributions, size-resolved concentrations, and source strengths, Aerosol Sci. Tech., 40, 348–360, doi:10.1080/02786820600612250, 2006.

Wallace, L. A., Emmerich, S. J., and Howard-Reed, C.: Source strengths of ultrafine and fine particles due to cooking with a gas stove, Environ. Sci. Technol., 38, 2304–2311, doi:10.1021/es0306260, 2004.

Wenzel, R. J., Liu, D.-Y., Edgerton, E. S., and Prather, K. A.: Aerosol time-of-flight mass spectrometry during the Atlanta Supersite Experiment: 2. Scaling procedures, J. Geophys. Res., 108, 8427, doi:10.1029/2001jd001563, 2003.

Zelenyuk, A., Yang, J., Song, C., Zaveri, R. A., and Imre, D.: "Depth-Profiling" and quantitative characterization of the size, composition, shape, density, and morphology of fine particles with SPLAT, a single-particle mass spectrometer, J. Phys. Chem. A, 112, 669–677, doi:10.1021/jp077308y, 2008.

Zhang, Q. J., Beekmann, M., Drewnick, F., Freutel, F., Schneider, J., Crippa, M., Prévôt, A. S. H., Baltensperger, U., Poulain, L., Wiedensohler, A., Sciare, J., Gros, V., Borbon, A., Colomb, A., Michoud, V., Doussin, J.-F., Denier van der Gon, H. A. C., Haeffelin, M., Dupont, J.-C., Siour, G., Petetin, H., Bessagnet, B., Pandis, S. N., Hodzic, A., Sanchez, O., Honoré, C., and Perrussel, O.: Formation of organic aerosol in the Paris region during the MEGAPOLI summer campaign: evaluation of the Volatility-Basis-Set approach within the CHIMERE model, Atmos. Chem. Phys. Discuss., 12, 29475–29533, doi:10.5194/acpd-12-29475-2012, 2012.

ACPD
13, 10345–10393, 2013

Table 1. Mass fractions of each chemical species determined for each ATOFMS class.

Species	K-EC	EC-OA	EC-OA-SO_x	EC-OA-NO_x	K-OA	K-OA-NO_x	K-OA-SO_x	OA-NO_x	OA-SO_x	OA-TMA
EC	0.57	0.62	0.21	0.32	0.14	0.06	0.05	0.07	0.08	0.04
OA	0.24	0.30	0.37	0.33	0.52	0.27	0.36	0.40	0.40	0.45
NH_4	0.06	0.01	0.04	0.06	0.02	0.07	0.13	0.17	0.11	0.21
SO_4	0.04	0.06	0.33	0.06	0.09	0.07	0.23	0.09	0.31	0.12
NO_3	0.08	0.02	0.05	0.23	0.21	0.52	0.22	0.27	0.10	0.17
K	0.02	< 0.01	< 0.01	< 0.01	0.02	0.01	< 0.01	< 0.01	< 0.01	< 0.01

ACPD
13, 10345–10393, 2013

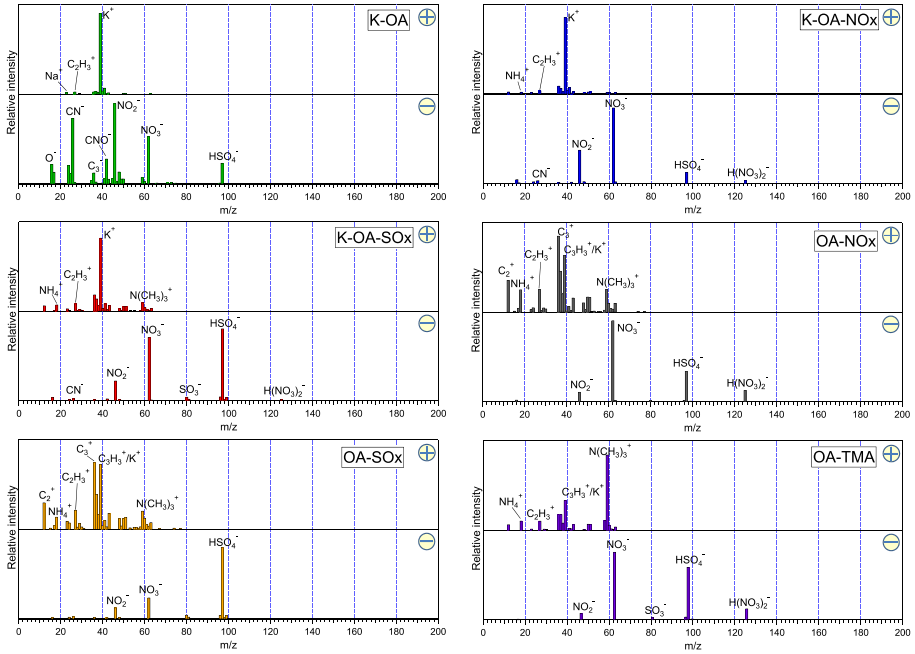

Fig. 1. Average single particle mass spectra for the ATOFMS OA classes.

ACPD
13, 10345–10393, 2013

Quantitative determination of carbonaceous particle mixing state

R. M. Healy et al.

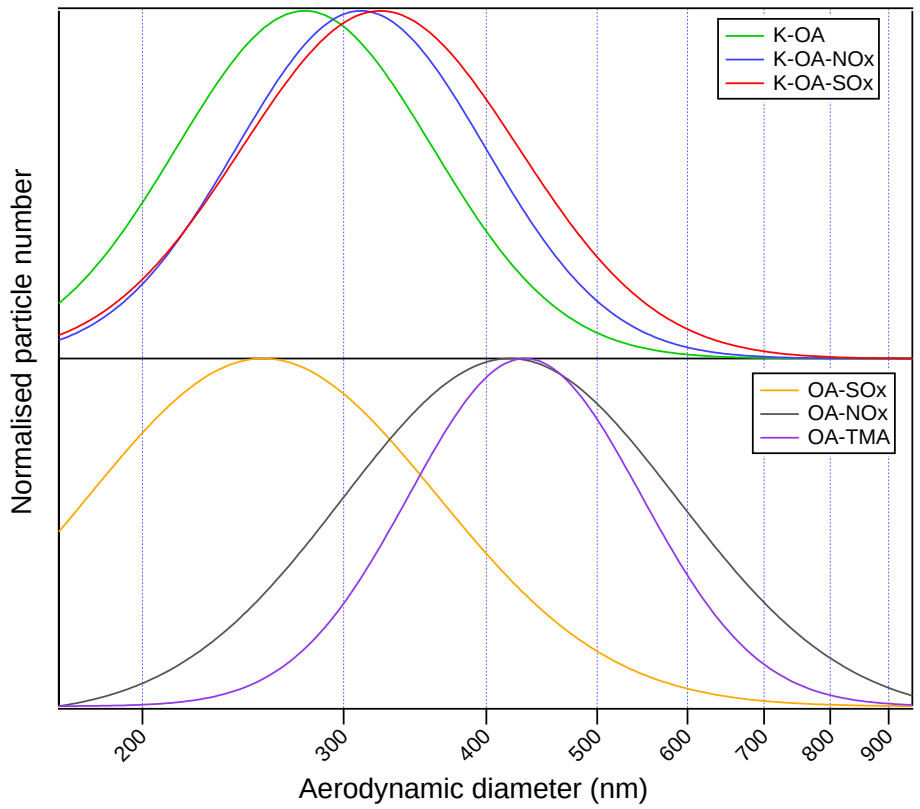

Fig. 2. Normalised lognormal fit of number-size distributions for the ATOFMS OA particle classes.

ACPD
13, 10345–10393, 2013

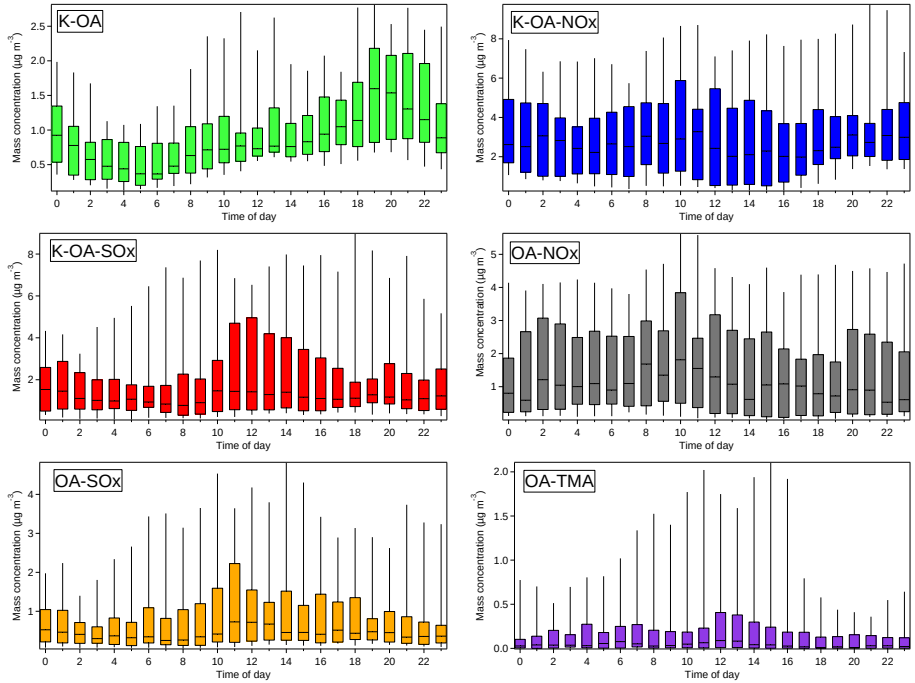

Fig. 3. Diurnal trends of mass concentrations for the ATOFMS OA particle classes ($N = 27$). Median, 75th percentile and 90th percentile are denoted by the solid line, box and whisker, respectively.

ACPD
13, 10345–10393, 2013

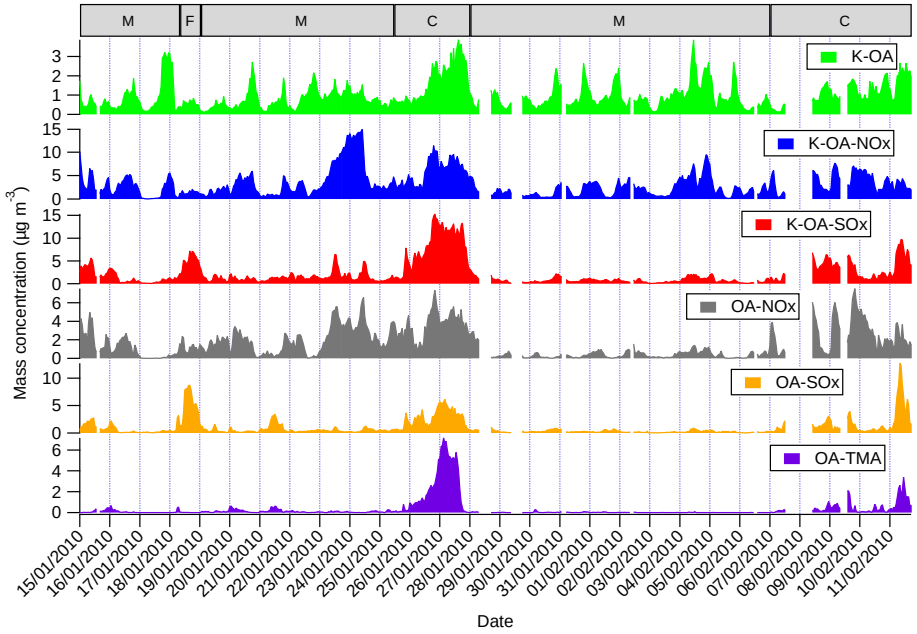

Fig. 4. Temporal trends for the ATOFMS OA particle classes. M, C and F correspond to periods influenced by marine air masses, continental air masses and fog, respectively.

ACPD
13, 10345–10393, 2013

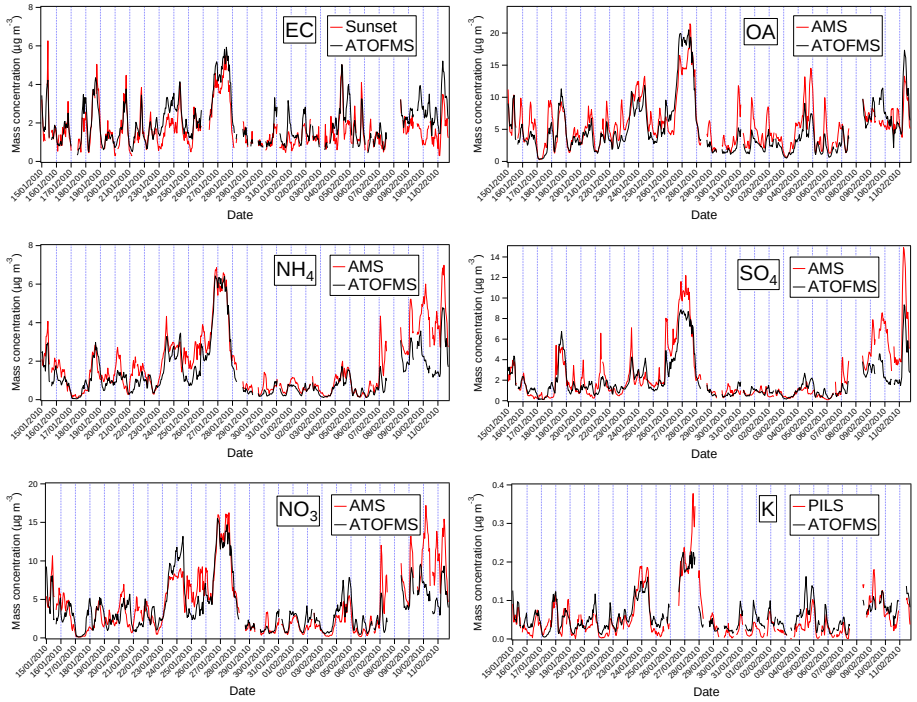

Fig. 5. Comparison of ATOFMS-derived, HR-ToF-AMS, PILS-IC and Sunset OCEC analyzer mass concentrations for organic aerosol (OA), elemental carbon (EC) and inorganic ions.

ACPD
13, 10345–10393, 2013

Quantitative determination of carbonaceous particle mixing state

R. M. Healy et al.

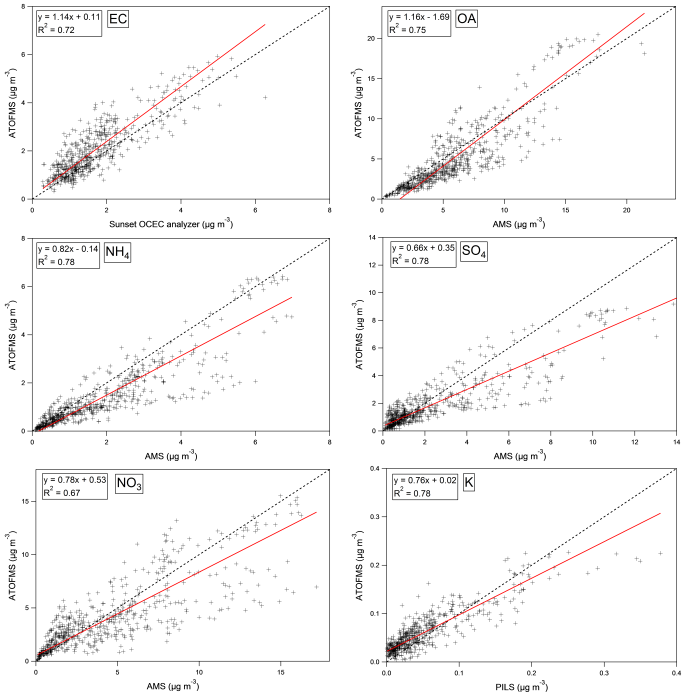

Fig. 6. Correlations for ATOFMS-derived mass concentrations for organic aerosol (OA), elemental carbon (EC) and inorganic ions and HR-ToF-AMS, PILS-IC and Sunset OCEC analyser data (N = 501). Red lines represent the orthogonal distance regression fit and black dashed lines indicate the 1 : 1 ratio.

ACPD
13, 10345–10393, 2013

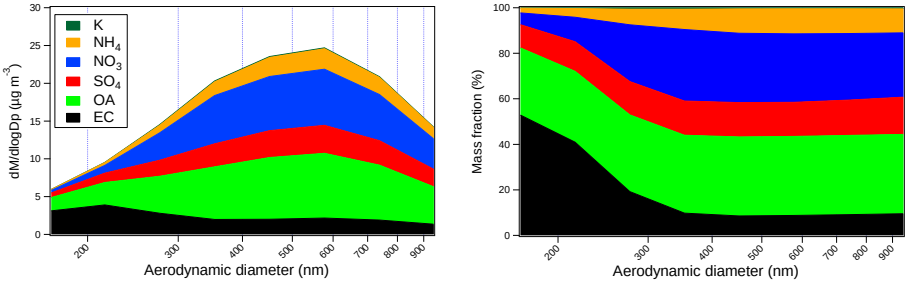

Fig. 7. Mass-size distributions (left, stacked) and size resolved average mass fractions (right, stacked) for each chemical species reconstructed using ATOFMS data. The relative contribution of potassium is very minor.

ACPD
13, 10345–10393, 2013

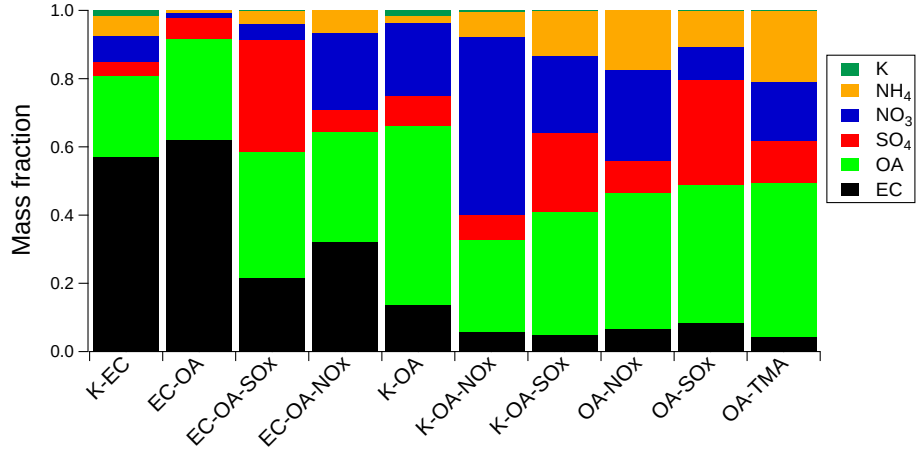

Fig. 8. Mass fractions of each chemical species determined for each ATOFMS class.

ACPD
13, 10345–10393, 2013

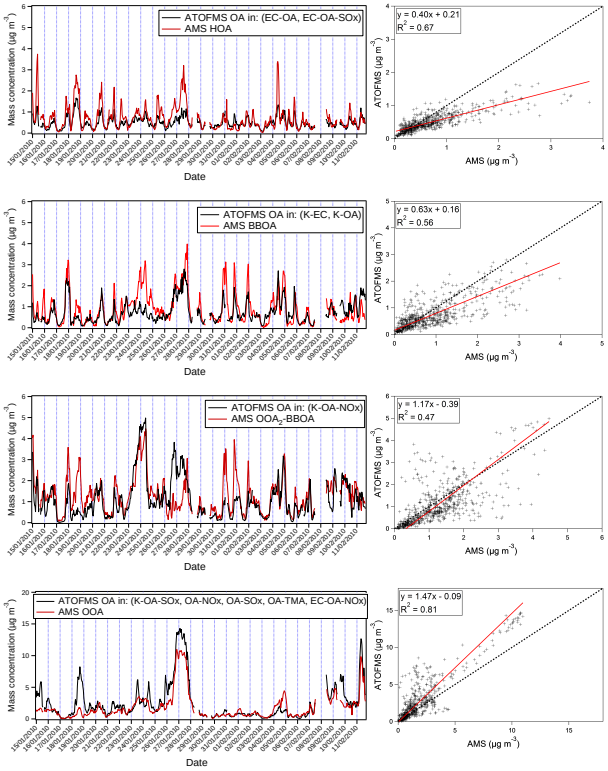

Fig. 9. Comparison of the HR-ToF-AMS OA PMF factors with mass concentrations of the OA content of selected ATOFMS single particle classes (N = 501). The red line represents the orthogonal distance regression fit and the black dashed line represents the 1 : 1 ratio.

ACPD
13, 10345–10393, 2013

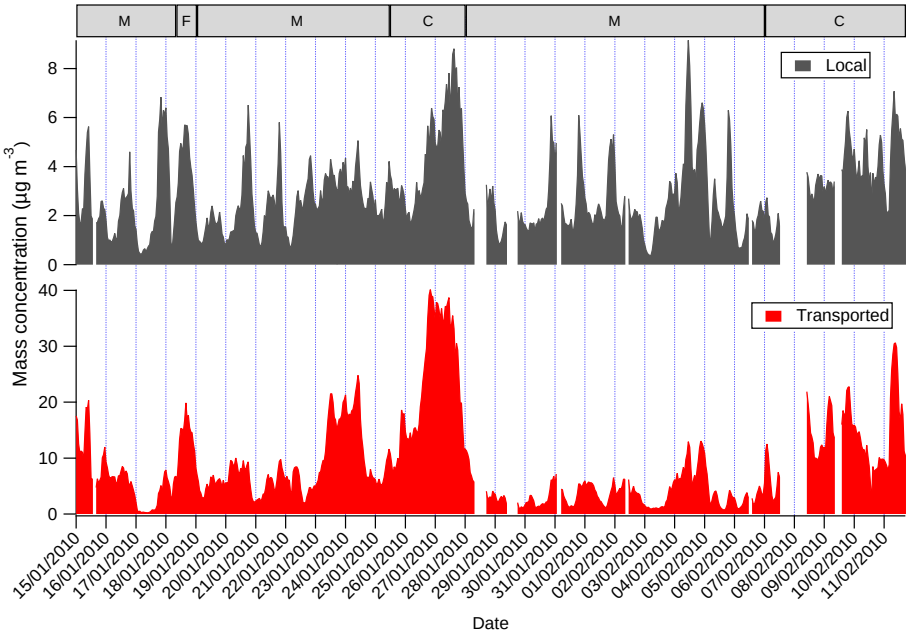

Fig. 10. Temporal trends for ATOFMS-derived particle mass apportioned to local and regional/continental sources. M, C and F correspond to periods influenced by marine air masses, continental air masses and fog, respectively.

ACPD
13, 10345–10393, 2013

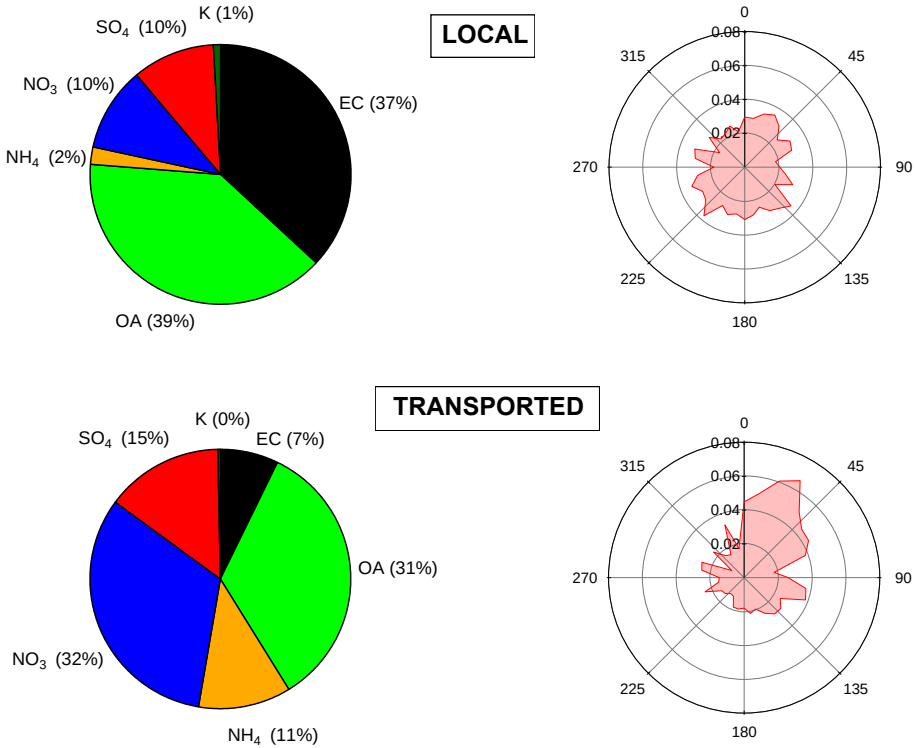

Fig. 11. Average ATOFMS-derived chemical composition and wind dependence for particles apportioned to local and regional/continental sources.

ACPD
13, 10345–10393, 2013

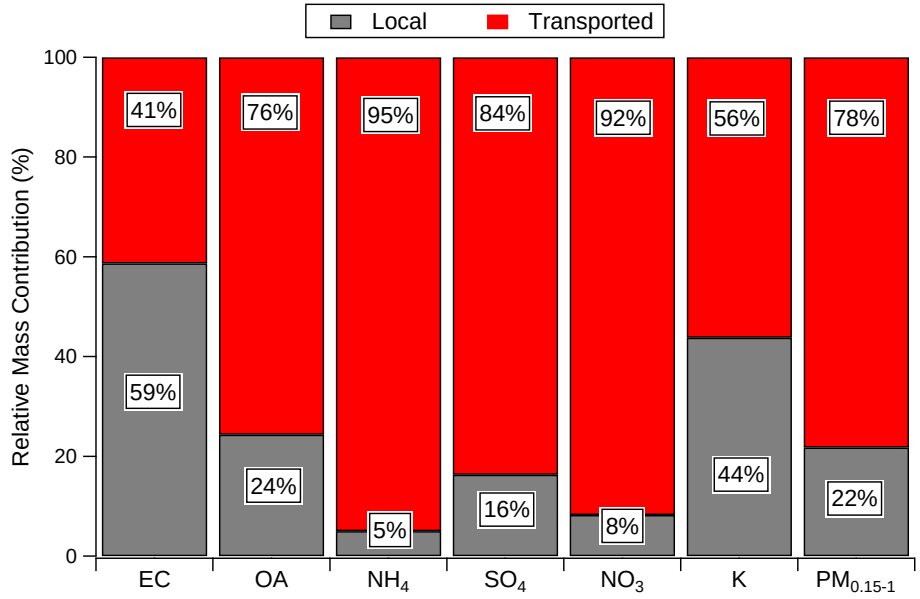

Fig. 12. Estimated relative mass contributions (%) of local and regional/continental scale emissions to each chemical species and reconstructed PM mass in the size range investigated.

ACPD
13, 10345–10393, 2013